Tone Detection Via Incoherent Averaging of Fourier Transforms to Support the Automated Spacecraft-Monitoring Concept

G. Lanyi and R. Kahn
Tracking Systems and Applications Section

An algorithm is presented for detection of very weak spacecraft tones generated by an onboard auxiliary oscillator with stability specifications similar to those of the small deep space transponder. Signal power is evaluated via discrete Fourier transforms, and detection is determined by comparing the measured power with a predetermined threshold. Limited oscillator stability precludes coherent integration of the signal over time scales longer than a few seconds; thus, the Fourier transform is performed independently on successive segments of data. Resulting power spectra are then averaged; potential frequency drift is accounted for by shifting the spectra when forming the average. The detection scheme is well suited to the proposed automated spacecraft monitoring system, in which a spacecraft sends a carrier signal modulated with one of four subcarrier frequencies to indicate the spacecraft's current state. Analysis based on theory and measurements indicates that reliable detection in a 1000-s interval can be achieved at a power signal-to-noise-density level, P/N_0, as low as -1 dB-Hz.

I. Introduction

The automated spacecraft monitoring system (ASMS)[1] is a proposed system for performing low-cost multispacecraft monitoring in an era when a multitude of small spacecraft missions will create high demand for ground tracking resources.[2] Under the current spacecraft-tracking paradigm, large (34-m to 70-m) antennas with very low-noise amplifiers track interplanetary spacecraft for many hours at a time, even during cruise phases of missions when data return is minimal. The spirit of the ASMS is to dramatically reduce tracking time and the use of the largest ground antennas during mission phases in which high-rate data return is not required. Also, the automated nature of the detection combined with simplified scheduling of antenna tracking should reduce the cost of Deep Space Network (DSN) operations.

In order to enable the use of smaller antennas, a simple signaling scheme is envisioned: The spacecraft transmits a message consisting of a carrier signal modulated by a square-wave subcarrier at one of four

[1] Also referred to as a beacon-monitoring or detection system.

[2] T. Peng and M. Sue, "Automatic S/C Monitoring Study," Study Outline (internal document), Jet Propulsion Laboratory, Pasadena, California, January 25, 1996.

known frequencies. Each of the four possible modulating frequencies represents a status of the spacecraft; thus, to interpret the message, the receiver must determine which of the four frequencies is modulating the carrier. The goal is to perform this signal detection using a dedicated antenna that could be a current 34-m or smaller ($\geq$5-m) antenna, in a time period of 20 minutes or less. Allowing another 20 minutes for slewing and postprocessing, a single receiver may be able to monitor at least 36 probes in a 24-hour period. Spacecraft that transmit messages indicating that they are in trouble or that they need to transmit data would subsequently be scheduled for tracking with a larger (34-m or 70-m) DSN antenna, at which time the spacecraft would modulate the subcarrier with telemetry in the usual manner.

The increased emphasis on low-cost interplanetary missions suggests that most future spacecraft will not be equipped with ultrastable oscillators. As a result, the frequency of a transmitted signal will exhibit significant short-term jitter and may drift by tens of Hertz or more during a 20-minute period. The oscillator instability, together with the low signal-to-noise ratio resulting from a combination of low transmitted power, low spacecraft antenna gain, low ground antenna gain, and relatively high receiver noise temperature on the ground, presents a challenge to the signal detection algorithm.

This article describes an algorithm designed to enable reliable signal detection by comparing the measured signal power to a predetermined threshold. Discrete Fourier transforms (DFTs) provide an approximate measure of received signal power as a function of frequency; consequently, the detection method also yields the signal frequency. This type of approximation of the power spectrum traditionally is referred to as a periodogram. The fast Fourier transform (FFT) algorithm is employed for efficient implementation of the discrete Fourier transforms. The final power spectrum is obtained by averaging a sequence of short-duration (typically up to a few seconds) power spectra. Because of oscillator instability, Fourier transforms cannot be performed over longer time intervals; the spacing of the frequency search must exceed the frequency-jitter range of the oscillator for a given integration time, and this constraint translates to an upper bound on coherent integration times. For a sufficiently strong signal, an integration time of a few seconds is adequate to detect the signal with high confidence. On the other hand, for weak signals, such as those envisioned for the ASMS system, the probability of detection is too low at such short integration times. In this case, however, the detection performance can be improved significantly by averaging the power of a series of disjoint Fourier transforms. In order to account for the frequency drift, the Fourier spectra must be aligned properly prior to averaging.

The performance of the detection algorithm depends on the success rate of discrimination between the signal power and the thermal noise of the receiver system. Therefore, probabilistic measures must be used for performance goals. We apply a form of the Neyman–Pearson criteria [1–3] for detection threshold determination; performance is characterized by computing the signal-to-noise threshold required to attain specified probabilities of false alarm, while optimizing the probability of detection. The threshold, once determined from a specific probability of false alarm, imposes a constraint on the total communication link budget: The spacecraft transmitted power, spacecraft and ground antenna gains, receiver noise temperature, and spacecraft–Earth range must yield a received signal whose power-to-noise ratio exceeds the threshold with a given value of detection probability. In this probabilistic detection scheme, it is assumed that the signal tone always is present within the boundaries of the frequency range under consideration. It should be noted that a detection of the tone also determines the tone frequency.

The outlined detection algorithm can be implemented purely in software or in a combination of software and hardware devices. In general, the data must be prepared and collected before the detection algorithm is applied. The radio-frequency spacecraft signal is downconverted to an intermediate frequency, digitized, downconverted again, and filtered to a baseband channel that is sufficiently narrow to ease the computational burden but wide enough to encompass uncertainty in the spacecraft frequency. The data stream preparation and the implementation of the detection algorithm may be carried out in several ways. A future demonstration will make use of the

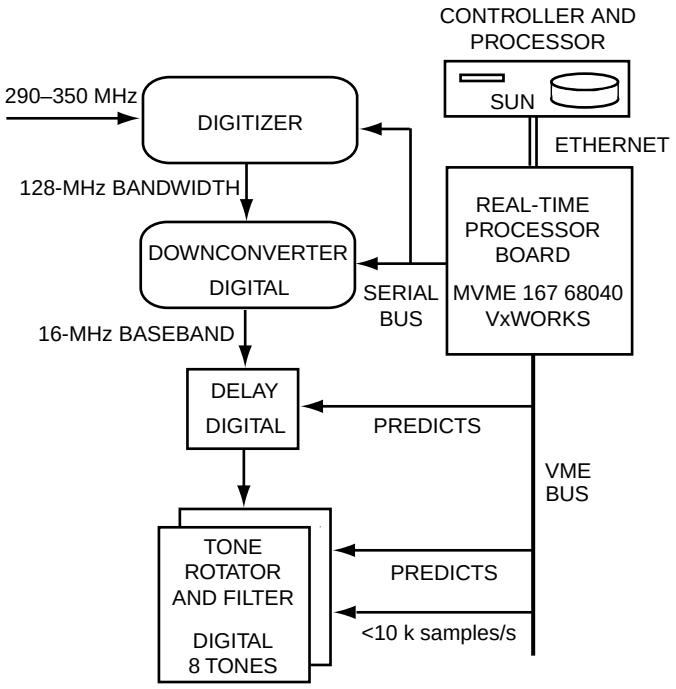

Fig. 1. Block diagram of the full spectrum recorder.

Full Spectrum Recorder (FSR) developed by the Jet Propulsion Laboratory (JPL) (Fig. 1);[3] the FSR will handle the data collection and processing to perform actual spacecraft status detection. In this case, the carrier radio frequency first is downconverted to an intermediate ($\approx$ 300-MHz) frequency; then the FSR digitally samples at 256 MHz and downconverts the signal to 2- to 10-kHz baseband channels using digital filters and a programmable oscillator as the mixing reference. The mixing frequencies are calculated from predictions of the received spacecraft frequency. The detection software residing on the control computer then processes the data in near-real time.

Before a detailed discussion of the algorithm is presented, a review of the relevant background information is in order. Most of the principles applied in this article were developed for radar signal detection during and shortly after World War II. An excellent exposition of the subject can be found in [4]. A more recent scientific application of the spectral power detection method was used in the Search for Extraterrestrial Intelligence (SETI) project [5] for low signal-to-noise levels. Recent related analyses originated at JPL include studies of fast Fourier transform efficiency for the Experimental Tone Tracker (ETT),[4] Fourier power summing for very long baseline interferometry (VLBI) and spacecraft-tracking application [6],[5] a cursory examination of ASMS detection efficiency by Kinman,[6] and a more elaborate study of probabilistic detection schemes [7]. In the absence of a firm estimate of the signal-to-noise-ratio threshold, JPL ASMS studies continued. The research presented in this article is based on the Fourier

[3] *DSCC Galileo Telemetry Subsystem, Functional Design and Software Requirements Document*, TDA/DSN 834-43, JPL D-11226 (internal document), Jet Propulsion Laboratory, Pasadena, California, December 21, 1993.

[4] S. A. Stephens, "An Analysis of FFT Tone Acquisition," JPL Interoffice Memorandum 335.1-92-14 (internal document), Jet Propulsion Laboratory, Pasadena, California, May 14, 1992.

[5] R. Kahn, "A Note on the Advantage Gained by Combining DFT Amplitudes From Several Channels When Conducting a Fringe Search With Block I VLBI Data," JPL Interoffice Memorandum 335.1-92-29 (internal document), Jet Propulsion Laboratory, Pasadena, California, October 12, 1992.

[6] P. Kinman,"Very Low Rate Noncoherent Frequency-Shift Signaling," JPL Interoffice Memorandum (internal document), Jet Propulsion Laboratory, Pasadena, California, December 14, 1995.

power averaging detection method[7] and initially adapted computer code written by J. Border for the Earth-based detection of the Galileo probe signal [8]. Some of the findings of this article were included in an internal document.[8] A parallel investigation led to a recent report [9] examining several different detection strategies, the best of which is close both in principle and numerics to the results presented in this article for the case of an ideal detection of a jitter-free tone.

II. Detection Algorithm for a Single Power Spectrum

For simplicity, we first consider the detection of a single pure tone. Estimates of the required power-to-noise-density ratio for single-tone detection will be corrected later for the signal structure of the proposed ASMS system, which consists of a carrier modulated by a square wave at four possible subcarrier frequencies (see Appendix A).

Signal detection is performed by selecting a threshold power, η, that is large enough so that the noise power at frequencies with no signal power present does not often exceed η, yet small enough so that the power at the signal frequency exceeds η with high probability.[9] The first task is to determine these probabilities for detection via a single Fourier transform.

As defined in Appendix C, the probability distribution of the noise amplitudes $a(\nu_k)$ and $b(\nu_k)$ at a frequency ν_k is a two-dimensional, central and symmetric, Gaussian distribution with a variance of σ^2. Thus, the probability distribution of the spectral power at a Fourier frequency associated only with noise is described as a χ^2 random variable with two degrees of freedom. Therefore, the probability of false alarm P_F, i.e., the probability that the noise power P_n exceeds a power-detection threshold η, may be written as

$$P_F \equiv \mathrm{P}(P_n > \eta) = \int_{\eta/\sigma^2}^{\infty} dy\, e^{-y} = e^{-\eta/\sigma^2} \tag{1}$$

The spectral power P_{s+n} at the signal frequency may be described as a noncentral χ^2 random variable with two degrees of freedom. The corresponding probability distribution is called a Ricean distribution, after S. O. Rice, who studied the bivariate Gaussian distribution extensively for signal processing [10]. It can be shown that the probability of detection P_D, i.e., the probability that the spectral power P_{s+n} at the Fourier frequency of the signal, in the presence of noise, exceeds threshold η, is

$$P_D \equiv \mathrm{P}(P_{s+n} > \eta) = \int_{\eta/\sigma^2}^{\infty} dy\, e^{-(y+y_0)} I_0(2\sqrt{yy_0}) \tag{2}$$

where y_0 is the power signal-to-noise ratio at the signal tone frequency,

---

[7] R. Kahn and G. Lanyi, "Proposal to Study 'Quick Look' Signal Detection for the Automatic Spacecraft Monitoring System," JPL Interoffice Memorandum (internal document), Jet Propulsion Laboratory, Pasadena, California, January 29, 1996.

[8] R. Kahn and G. Lanyi, "Automatic Spacecraft Monitoring Concept Demonstration Progress Report," JPL Interoffice Memorandum 335.1-96-10 (internal document), Jet Propulsion Laboratory, Pasadena, California, May 30, 1996. See also M. K. Sue, R. Kahn, G. Lanyi, V. Vilnrotter, M. Simon, and T. Peng, *Automated Spacecraft Monitoring System (ASMS) Study Report*, JPL D-14396 (internal document), Jet Propulsion Laboratory, Pasadena, California, March 15, 1997.

[9] A list of the symbols used throughout this article is provided in Appendix B.

$$y_0 = \frac{P_s}{N_0} T \tag{3}$$

$I_0(z)$ denotes the modified Bessel function of zeroth order [11], P_s is the signal power, T is the integration time of the Fourier transform, and N_0 denotes the constant spectral density of thermal noise. The complement of P_D is the probability of missed detection:

$$P_M = 1 - P_D \tag{4}$$

Equation (1) defines the probability of false alarm at a single Fourier frequency. One can also define a probability of false alarm occurring anywhere within the entire frequency search range. This is the probability of a false detection, P_{false}, i.e., the probability that the noise power exceeds the threshold η at any frequency in the Fourier spectrum, other than the frequency under consideration for detection. Given n frequencies and n independent samples, the probability that the noise power at least at one of the $n-1$ frequencies exceeds the threshold η is $P_{false} = 1-(1-P_F)^{(n-1)}$. In the ASMS detection scheme described in Section I and Appendix A, a message tone can be present in any of four frequency bands, each containing N Fourier frequencies. Thus, $n = 4N$ and, consequently,

$$P_{false} = 1 - (1 - P_F)^{(n-1)} = 1 - (1 - P_F)^{4N-1} \tag{5}$$

In the above discussions, the signal frequency has been assumed to correspond to one of the Fourier frequencies. In general, the tone lies between the discrete Fourier frequencies and drifts during the integration. As a result, the power spectrum of the tone spreads over all Fourier frequencies, and thus the observed peak spectral power is less than the original power of the tone. To find a better approximation of the peak power, either the Fourier transform of the tone is interpolated by employing the method of "zero padding" or the tone frequency is shifted closer to the Fourier frequency. Both of these methods are described in Appendix D. With these improvements, there still remains a signal power loss due to the frequency drift; this effect will be discussed below.

The ASMS assumptions defined in Appendix A can be applied to yield an estimate of required power signal-to-noise-ratio level for reliable detection. For a frequency uncertainty of ± 1 kHz, the sampling interval T_s must be $\leq 1/2000$ s.[10] The coherent integration time of the Fourier transform, $T = NT_s$, must be small enough so that the tone is not allowed to drift beyond a single Fourier frequency spacing, $\Delta\nu$, during the integration period, T. Actually, this condition is not optimal, because the power loss is 4 dB at the extremes of the frequency spacing (Appendix D). To keep the mean loss within a few tenths of a dB, the drift range must be on the order of $\Delta\nu/2$. The actual *linear* drift range is half of this value and thus $\Delta\nu/4$, since the linear-drift function is centered at the Fourier frequency (see Footnote 17 in Appendix E). This condition restricts the integration time T; the estimation of T and a calculation of the corresponding power losses are presented in Appendix E. With the given ASMS specification of oscilllator noise levels and linear drift limits, the result is that T must be near 1 s, and at $T = 1$ s, the power loss due to frequency drifts is $\approx$0.45 dB. Given that $T_s = 1/2000$, our current choice of $T = 1$ s corresponds to $N = 2000$ terms in the Fourier sum.

Summarizing the results, Fig. 2 plots the probability of missed detection, P_M, against the probability of false detection with $N = 2000$ at fixed power signal-to-noise levels $(P/N_0)T$. For the duration of $T = 1$ s, the required P/N_0 is $\approx$16 dB-Hz at the probability values chosen in Section VII: $P_{false} = P_M = 5 \times 10^{-4}$.

[10] This corresponds to a sampling rate less than or equal to the half Nyquist rate, because the baseband data stream is complex valued.

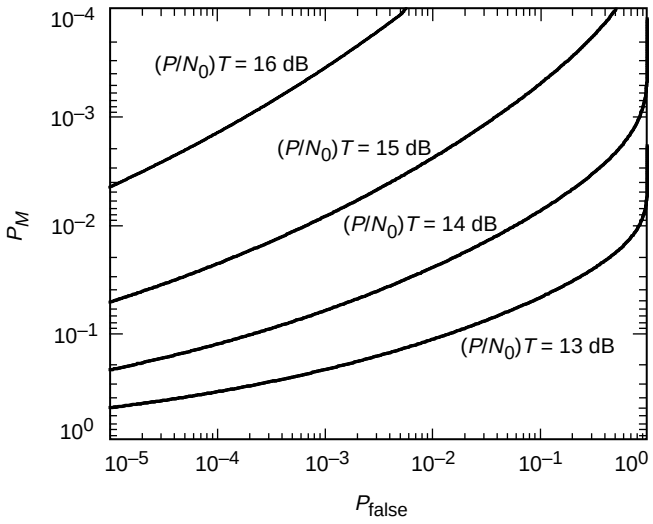

Fig. 2. Missed detection probability versus false alarm probability for a single *T*-sec DFT for several power-to-noise ratios, $(P/N_0)T$. False alarm probabilities are computed assuming 8000 Fourier frequencies.

III. Incoherent Average of Power Spectra

In order to detect a fixed-frequency signal via Fourier transform, it generally is best to integrate coherently as long as possible to obtain the highest possible signal-to-noise ratio. The integration time is limited, however, by signal-frequency variations, which cause amplitude loss and imprecise signal-frequency determination. As discussed above, these effects can be reduced by choosing an integration time short enough so that the frequency variation over the integration interval remains smaller than the frequency spacing of the Fourier transform. Of course, a shorter integration leads to a higher thermal noise level and, thus, to a lower signal-to-noise ratio. The variation of the noise level about its mean value, however, can be decreased to a desired level by averaging the resulting power spectra over a sufficiently long time period. The reduction in noise level variation, in turn, improves the detectability of the signal.

This process is illustrated in Fig. 3 for a Fourier integration time of 1 s. In this figure, the power level is normalized to unity, and the power signal-to-noise ratio is chosen to be 1 dB. The figure shows that, under incoherent power averaging, the mean level of the noise is constant, while the fluctuations about the mean decrease as a function of integration time. However, the rate of decrease of the fluctuations ($\propto 1/\sqrt{T}$) is not as steep as the rate at which the mean noise power and its variation ($\propto 1/T$) would decrease if the Fourier transform could be extended for a longer time. Still, this effect makes it possible to distinguish the signal from the noise with arbitrary certainty at sufficiently long observing times, if the observed tone frequency is perfectly constant. Note, however, that detection by incoherent power summing is not as efficient as detection via coherent integration, and the phase of the signal cannot be determined in this way. It should also be pointed out that either averaging or summing of the power leads to the same detection criteria if the detection thresholds are defined consistently. In this article, both terminologies are used interchangeably; the probability formulas below refer to the sum of powers, conforming to the literature.

Because of the frequency drift of the signal, the sequential power spectra must be aligned properly in the frequency space; this procedure is discussed in the following section. Given the aligned power spectra, one may consider a signal with constant tone frequency. We assume a sequence of M power spectra and calculate the summed power at each frequency. The composite probability distribution of

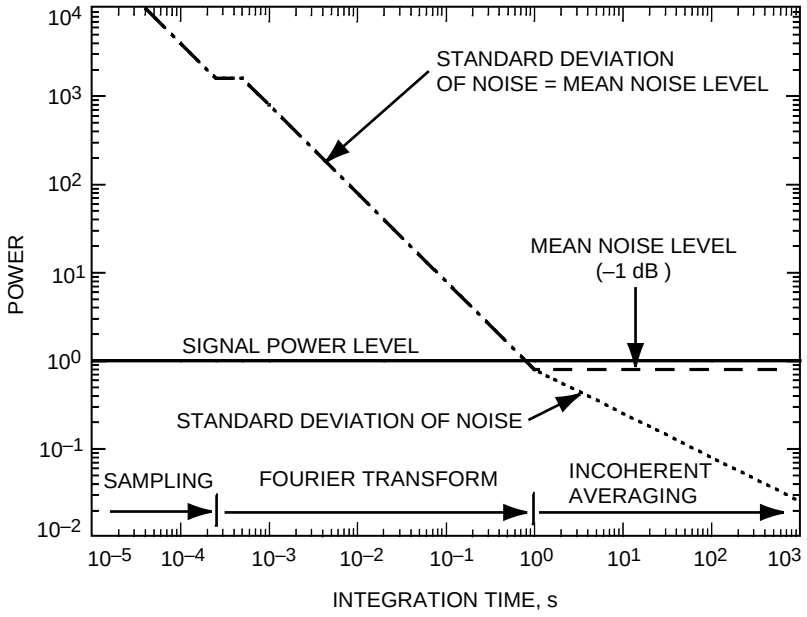

Fig. 3. Power noise levels versus integration time. The integration time refers to three different processes: sampling, Fourier transform, and incoherent average of Fourier spectra.

the noise amplitudes $a(\nu_k)$ and $b(\nu_k)$ for each frequency is now a $2M$-dimensional Gaussian distribution, and the probability distribution of the sum of the noise power is a χ^2 distribution with $2M$ degrees of freedom. It follows then that the probability of false detection P_F, i.e., that the total noise power P_n exceeds a total power threshold of η_M, is

$$P_F \equiv \mathrm{P}(P_n > \eta_M) = \int_{\eta_M/\sigma^2}^{\infty} dy\, e^{-y}\, \frac{y^{\,M-1}}{(M-1)!} = e^{-\eta_M/\sigma^2} \sum_{k=0}^{M-1} \frac{(\eta_M/\sigma^2)^k}{k!} \tag{6}$$

The probability distribution for the M-fold sum of the signal-plus-noise power is now a noncentral χ^2 distribution with $2M$ degrees of freedom [12]. Consequently, the probability of detection, P_D, i.e., the total signal-plus-noise power, P_{s+n}, exceeds the threshold, η_M, is [13,14]

$$P_D \equiv \mathrm{P}(P_{s+n} > \eta_M) = \int_{\eta_M/\sigma^2}^{\infty} dy\, e^{-(y+y_{0M})} \left(\frac{y}{y_{0M}}\right)^{(M-1)/2} I_{M-1}(2\sqrt{y y_{0M}}) \tag{7}$$

where $I_{M-1}(z)$ denotes the modified Bessel function of $M-1$ order and the total power signal-to-noise ratio, y_{0M}, is now

$$y_{0M} = M \frac{P_s}{N_0} T \tag{8}$$

For power averaging, instead of power summing, similar formulas can be derived, corresponding to normalized χ^2 probability distributions. The probability of false detection, P_{false}, is unaffected by either power summing or averaging. However, it *is* modified by the increased search space resulting from the unknown drift. Thus, the exponent n in Eq. (5) is given by $n = 4NN_r$, where N_r represents the number

of linear frequency drift rates under consideration.[11] Therefore, the probability of false detection, in the presence of frequency-drift-rate search, becomes

$$P_{false} = 1 - (1 - P_F)^{4NN_r - 1} \tag{9}$$

Numerical results of this section are presented in Figs. 4 and 5. These figures plot the missed-detection probability against the false-detection probability for incoherent power sums of 100 and 1000 Fourier transforms for $N = 2000$ Fourier frequencies, $N_r = 100$ frequency rates, and a range of power signal-to-noise ratios $(P/N_0)T$. For an integration time of $T = 1$ s, these correspond to a detection over 100 or 1000 s. A comparison of these figures to Fig. 2 shows how the power signal-to-noise ratio, $(P/N_0)T$, required to attain the same receiver performance is lowered by summing the individual signal powers.

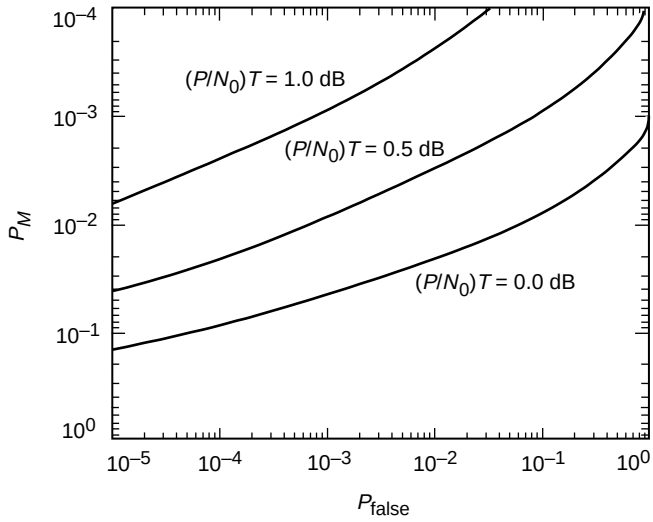

Fig. 4. Missed detection probability versus false alarm probability for incoherent sums of 100 *T*-sec DFTs for several power-to-noise ratios, $(P/N_0)T$. False alarm probabilities are computed assuming 8000 Fourier frequencies and 100 drift rates.

IV. Power Spectra Alignment

The frequency drift of the signal limits coherence time and, therefore, we resort to averaging of the power spectra. In order to carry out the averaging, the frequency drift must be modeled and removed. This can be done before the Fourier transform [9] or after the Fourier transform. Each method has advantages and disadvantages, as described below. The frequency drift model is chosen to be a polynomial model; in its simplest form, it consists of a linear drift model. The model parameters are determined by a systematic search: The optimum parameters correspond to the maximum detected signal power. If the model is applied before the Fourier transform, then the model is a truly continuous function of time, and the model drift is perfectly removed, but the Fourier transforms have to be performed for all necessary values of model parameters under consideration; thus, the method can be computationally laborious. If

[11] This relation is exact only for uncorrelated search paths in the time–frequency space. For the actual search space, the equivalent value of n is smaller. The use of a larger value, however, results in a conservative over-estimate of the required power signal-to-noise ratio for a given pair of probabilities of false and missed detections. This effect is relatively small; reducing n by a factor of 3 decreases the required power signal-to-noise ratio by 0.2 dB in the case of Fig. 5.

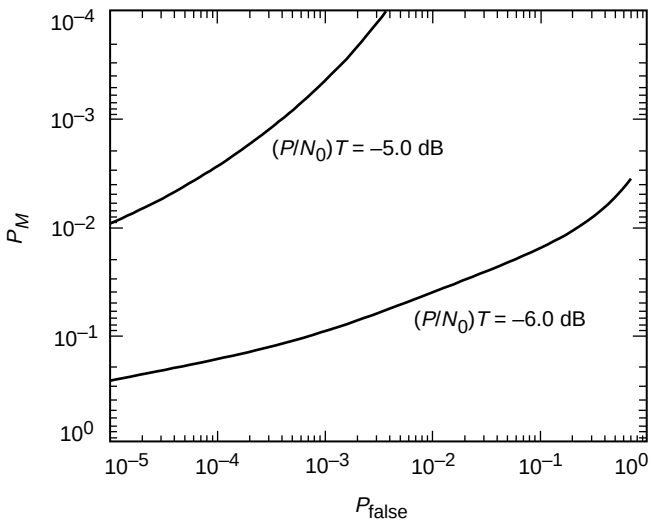

Fig. 5. Missed detection probability versus false alarm probability for incoherent sums of 1000 *T*-sec DFTs, using 100 linear drift rate searches for summing the power of 1000 individual DFTs. False alarm probabilities are computed assuming 8000 Fourier frequencies and 100 drift rates.

we apply the model after the Fourier transforms, then the model is discontinuous, due to the nature of discrete Fourier transforms, there is some loss of signal power. However, in this case, a set of Fourier transforms is performed only once, and the search for the optimum parameters is performed on this single set of Fourier transforms. Since a real- or near-real-time detection is strongly preferred, only the latter method is discussed in this article; it is computationally faster than the former case. Also, in the ASMS case, the major power loss (≈0.3 dB) is due to the changing displacement of the signal frequency with respect to the Fourier frequencies over a sequence of Fourier transforms (Appendix D); the effect of the frequency drift within a single Fourier transform is negligible, 0.003 dB (Appendix E). Thus, there is no significant advantage to pre-Fourier-transform frequency modeling.

In this article, only a linear drift model is considered. The specified maximum drift rate is $\dot{\nu} = \pm 0.05$ Hz/s and, since the Fourier resolution is $\Delta\nu = 1$ Hz for an integration time of $T = 1$ s, an observation of 1000 s thus requires $N_r = 100$ discrete frequency rates in the frequency-rate search space to keep the maximum accumulated frequency error within half of the Fourier spacing.

V. Detection of Two Tones

In the proposed ASMS signal detection scheme, the carrier is modulated by a square wave at four possible subcarrier frequencies, producing a set of odd subharmonics centered around the carrier. If the carrier is fully suppressed, then 81 percent of the power resides in the first upper and lower harmonics. The upper and lower subharmonic tones cannot be coherently recombined in a direct fashion,[12] but an incoherent power sum of these tones still improves the detection performance.

Incoherent power summing is effective when the error of the known differential frequency between the upper and lower harmonics is sufficiently smaller than the resolution of the Fourier transform. If the differential frequency of the harmonics is uncertain relative to the Fourier spacing, the summed power is

[12] The unknown differential phase offset and phase noise limit the coherent recombination. A search in the differential phase domain would make recombination possible; thus, one could regain most of the 1-dB loss due to incoherent summing with a large computational overhead.

less than the sum of the theoretical peak powers. This power loss would be an addition to the power loss related to the noise statistics, which effect is described below. For the choice of $T = 1$ s, the frequency resolution is $\Delta\nu = 1$ Hz. Since the differential subcarrier frequency error given by the ASMS specification is 0.1 Hz (Appendix A), an incoherent recombination of the two harmonics is quite efficient.

To evaluate the power loss due to incoherent recombination of the two tones of equal power, we compare the power signal-to-noise ratios of a single and two summed tones to achieve comparable statistical performance. Figure 6 presents this comparison of receiver performance and also exhibits the performance when the same single-tone power is divided equally between two tones. The figure shows missed-detection probability versus false-detection probability for a 100-s observation of a single tone with $P/N_0 = 0$ dB-Hz, and for two tones each having $P/N_0 = -3$ dB-Hz. For a given false-detection probability, the probability of missed detection is more than ten times larger in the two-tone case. The two-tone combination scheme achieves performance comparable to the single-tone case if the summed $P/N_0 = 1$ dB-Hz, i.e., if the total transmitted power exceeds by 1 dB the power transmitted in the single-tone case.

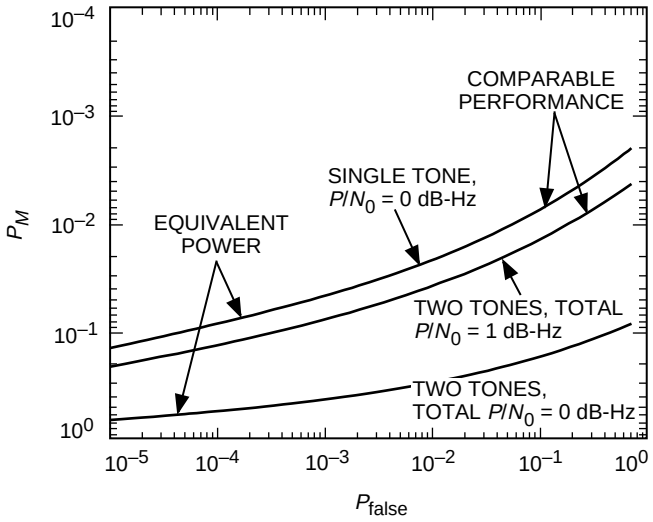

Fig. 6. A comparison of two-tone versus single-tone performance. The observation interval is 100 s; the DFT interval is 1 s. Spectra from two tones are summed incoherently. False alarm probabilities are computed assuming 8000 Fourier frequencies.

VI. Experimental Verification

In the above analysis, the analytic expressions for the false alarm and detection probabilities assume that the noise is white and Gaussian. The effect of oscillator instability was accounted for by limiting the duration of the Fourier transforms to a few seconds in order to maintain signal coherence. In reality, the oscillator may add a significant non-Gaussian non-white component to the underlying thermal noise. In order to gain better insight into the effect of oscillator instability on receiver performance and as a check on the theoretical detector performance calculations, data were acquired at a DSN test facility (DTF 21) using a full spectrum recorder to record a test signal generated at the Telecommunication Development Laboratory (TDL) using the Galileo spare auxiliary oscillator. The signal consisted of an 8.4-GHz (X-band) carrier modulated with a 22.5-kHz square-wave subcarrier. No telemetry data modulated the subcarrier. The FSR digitized the signal at an intermediate frequency of ≈300 MHz, downconverted the lowest eight harmonics ($\pm1, \pm3, \pm5, \pm7$) to separate 3200-Hz baseband channels, and recorded the digitized samples.

A plot of carrier frequency versus time as measured by the FSR is presented in Fig. 7. The largest local drift rate over the 1-hour time span is approximately 0.05 Hz/s; the root-mean-square fluctuation over 10-s intervals is 0.2 Hz. This is consistent with the expected stability of the small deep space transponder over comparable time intervals.

Attenuation of the input signal was varied over the approximately 1-hour-long observation to obtain data with a range of signal-to-noise ratios. During the final 19 minutes, the +7th harmonic had $P/N_0 = 1$ dB-Hz; these data were processed using the incoherent single-tone detection scheme presented above: Discrete Fourier transforms, with a 1-s integration time and zero-padding by a factor of two, were performed, and the 1-s spectra were summed using an ensemble of drift rates ranging from −0.05 Hz/s to +0.05 Hz/s.

In order to acquire statistics on detector performance, the data were partitioned into twenty-two 50-s subintervals, with independent detections performed on each subinterval. The relation between P_M and P_{false} was computed in the following manner: For a given detection threshold, P_{false} was calculated from the theoretical values of P_F given by Eq. (6), while σ^2 was determined from part of the data with ignorable signal content. Next, P_M was computed by counting the fraction of subintervals in which the signal power fell below the detection threshold. This result and the theoretical expectations based on Eqs. (6) and (7) are plotted in Fig. 8. This figure shows that the measured detector performance is degraded by approximately 1 dB relative to the theoretical performance. This appears to be a combination of five effects (most of which are estimated in Appendices D and E): (1) approximation of the frequency drift model with a discrete step-wise linear model mandated by the discrete Fourier transformation (−0.003 dB), (2) deviation from the linear frequency-drift model, (3) omission of the non-white oscillator noise from the theoretical calculations, (4) power loss due to tone-frequency fluctuation during Fourier integration time (−0.15 dB), and (5) power loss from tone misalignment relative to the Fourier frequency including the zero-padding effect (−0.3 dB). There is one more known source of error: omission of the effect of zero padding on the statistics of probabilities of missed and false detection. An analysis of this effect is not within the scope of this article. It should be noted, however, that low probabilities of missed detection are not much affected by zero padding and, thus, most likely are ignorable in the 1-dB power loss above. The estimated losses add up to 0.45 dB; thus, part of the 1-dB loss is explained qualitatively.

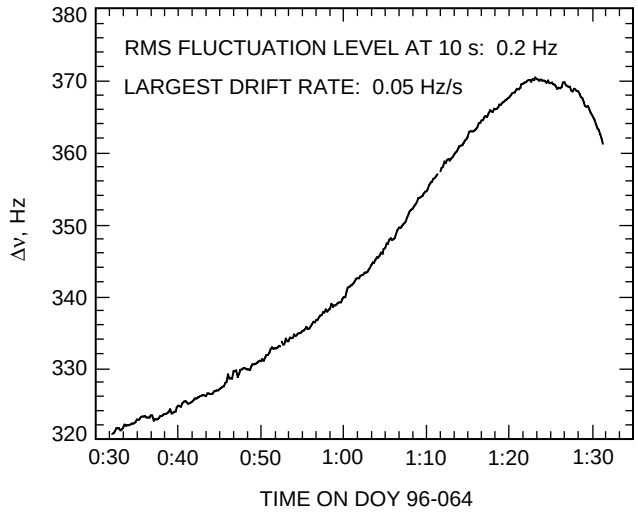

Fig. 7. Frequency drift of the Galileo auxiliary oscillator versus time, measured by the FSR at DTF 21. The frequency is measured at 10-s intervals.

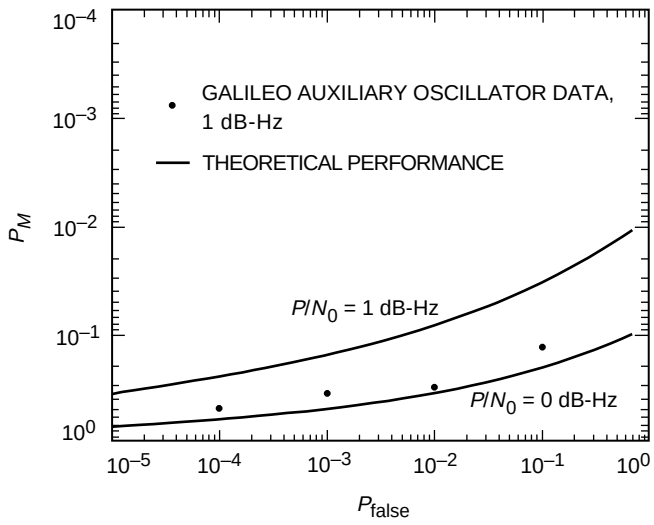

Fig. 8. Theoretical versus measured receiver performance for sums of 50 1-sec FFTs. False alarm probabilities are computed using 3200 Fourier frequencies and 10 drift rates.

Our final task is a projection of the measured 1-dB loss onto an observation of 1000 s. Since the frequency fluctuation of the oscillator noise is correlated over the observation interval, and this correlation is not perfectly removed by the process of summing the powers of Fourier transforms via spectrum alignment, the oscillator noise error of the averaged power is expected to be somewhat larger than that of a single Fourier transform. An evaluation of this power loss is fairly complex; our current rudimentary estimate gives an additional loss of 0.3 dB for a 1000-s observation.

Also, on larger time scales, nonlinear frequency drifts must be considered; thus, a polynomial model or quadratic spline is used to model the frequency drift. In extending a 50-s observation to a 1000-s observation, the duration of observation is increased twentyfold. However, the ASMS frequency-drift specification severely limits the range of polynomials that need be considered for alignment of the spectra. We estimate that the search space is not enlarged more than tenfold by using a low-order polynomial model. This expansion of the search space increases the false-detection probability; an estimated 0.3 dB is required to compensate for the performance degradation.

Summing the above effects, it is anticipated that the performance power loss for a 1000-s observation is larger than the 1-dB loss concluded from the 50-s observations by about 0.6 dB. As a precaution, we empirically increase the estimated performance loss to 2 dB for a 1000-s observation.

VII. Conclusion

In order to translate the above considerations into a practical spacecraft-detection scenario, performance criteria, i.e., the probabilities of false and missed detection, must be specified. Therefore, we assume a spacecraft with a lifetime of 3 years (≈1000 days) during which there are practically no false or missed detections. Observations are conducted daily. These conditions bound the false and missed probability values at the $1/1000 = 10^{-3}$ level. Therefore, we chose a value sufficiently below this level: $P_{false} = P_M = 5 \times 10^{-4}$.

Figure 5 indicates that the corresponding power signal-to-noise-density ratio is $P/N_0 \approx -5$ dB-Hz for detection of a single tone observed for 1000 s ($T = 1s, N = 2000, M = 1000$, and $N_r = 100$). This must be corrected by 1 dB if the power is distributed between two tones that are incoherently combined; also,

between 1 and 2 dB must be added to account for the previously discussed losses in the performance of the detection algorithm. Finally, an additional 0.9-dB correction is required to account for the fact that the actual signal is a square-wave modulated carrier and only the strongest two harmonics are retained. Thus, the requirement on the received P/N_0 is -1 dB-Hz.

Acknowledgments

The authors would like to acknowledge the support of the ASMS system design team leaders, Ted Peng and Miles Sue, and Jim Deweese for providing TDL support during acquisition of Galileo auxiliary oscillator data at DTF 21. We also appreciate the courtesy of Jim Border, who provided our initial software code. We also acknowledge the insight of Miles Sue and Victor Vilnrotter for pointing out the influence of the degrees of freedom associated with multiple message tones and frequency-rate space, respectively, on false detection probabilities. Thanks are also due to George Purcell for the careful reading of the manuscript of this article and for his valuable comments and corrections.

References

[1] J. Neyman and E. Pearson, "On the Problem of the Most Efficient Tests of Statistical Hypothesis," *Phil. Trans. Roy. Soc.*, vol. A 231, pp. 289–337, 1933.

[2] H. L. Van Trees, *Detection, Estimation, and Modulation Theory*, New York: John Wiley, 1968.

[3] M. K. Simon, S. M. Hinedi, and W. C. Lindsey, *Digital Communication Techniques*, Englewood Cliffs, New Jersey: Prentice Hall, 1995.

[4] J. V. DiFranco and W. L. Rubin, *Radar Detection*, Englewood Cliffs, New Jersey: Prentice Hall, 1968.

[5] M. Garyantes, M. Grimm, and H. Wilck, "A Wide-Band, High-Resolution Spectrum Analyzer," *Third Decennial US–USSR Conference on SETI*, edited by S. Shostak, Astronomical Society of the Pacific Conference Series, vol. 47, pp. 61–64, 1993.

[6] R. Kahn, S. Thurman, and C. Edwards, "In-Situ Radio-Metric Tracking to Support Navigation for Interplanetary Missions With Multiple Spacecraft," AAS Paper 93-164, *AAS/AIAA Spaceflight Mechanics Meeting*, Pasadena, California, February 22–24, 1993.

[7] M. K. Simon, M. M. Shihabi, and T. Moon, "Optimum Detection of Tones Transmitted by a Spacecraft," *The Telecommunications and Data Acquisition Progress Report 42-123, July–September 1995*, Jet Propulsion Laboratory, Pasadena, California, pp. 69–98, November 15, 1995.
http://tda.jpl.nasa.gov/tda/progress_report/42-123/123A.pdf

[8] W. M. Folkner, R. A. Preston, J. S. Border, J. Navarro, W. E. Wilson, and M. Oestreich, "Earth-Based Radio Tracking of the Galileo Probe for Jupiter Wind Estimation," *Science*, vol. 275, pp. 644–645, January 1997.

[9] M. K. Simon, V. Vilnrotter, A. Mileant, and S. Hinedi, "Optimum Strategies for Monitoring the Operational Status of a Spacecraft," *The Telecommunications and Data Acquisition Progress Report 42-127, July–September 1996*, Jet Propulsion Laboratory, Pasadena, California, pp. 1–51, November 15, 1996. http://tda.jpl.nasa.gov/tda/progress_report/42-127/127C.pdf

[10] S. O. Rice, "Mathematical Theory of Random Noise," *Bell System Tech. J.*, vol. 23, pp. 283–332, 1944; vol. 24, pp. 46–156, 1945; reprinted in *Selected Papers on Noise and Stochastic Processes*, edited by N. Wax, New York: Dover, pp. 133–294, 1954.

[11] G. N. Watson, *A Treatise on the Theory of Bessel Functions*, Cambridge: Cambridge University Press, 1962.

[12] M. Evans, N. Hastings, and B. Peacock, *Statistical Distributions*, New York: John Wiley, 1993.

[13] J. I. Marcum, "A Statistical Theory of Target Detection by Pulsed Radar," *Rand Report RM-754*, December 1947; reprinted in *Trans. IRE Prof. Group on Information Theory*, vol. IT-6, pp. 59–144, April 1960.

[14] J. I. Marcum, "A Statistical Theory of Target Detection by Pulsed Radar, Mathematical Appendix," *Rand Report RM-753*, July 1948; reprinted in *Trans. IRE Prof. Group on Information Theory*, vol. IT-6, pp. 145–267, April 1960.

Appendix A
Study Assumptions

Table A-1 lists a set of assumptions that have guided the algorithm development.[13] It is assumed that the signal structure consists of a carrier signal frequency modulated by a square-wave subcarrier, with no additional modulation on the subcarrier. The spacecraft may use any of four different subcarriers to modulate the carrier. The resulting signal spectrum is a set of delta functions located at $\nu_c + n\nu_{sc}$, where $n = 0, \pm 1, \pm 3, \pm 5, \ldots, \nu_c$ is the carrier frequency and ν_{sc} is the subcarrier frequency. The power in each subcarrier tone is inversely proportional to the square of the harmonic number; if the carrier is fully suppressed, then 81 percent of the transmitted power resides in the upper 1st and lower 1st subcarrier harmonic. Processing only these first harmonics reduces the required bandwidth of the receiver, while sacrificing approximately 0.9 dB of the available power.

Table A-1. Assumptions for the algorithm development.

Parameter	Description
Signal structure	Carrier modulated with square-wave subcarrier
Signaling scheme	Four different subcarrier frequencies
Carrier frequency	8.4 GHz (suppressed)
Carrier frequency uncertainty	±1 kHz/48 h
Subcarrier relative stability	0.1 Hz
Observable frequencies	First harmonics of the four subcarriers $\pm 20, \pm 25, \pm 30, \pm 35$ kHz
Duration of observation	One observation/day, 20 min maximum
Oscillator drift range (maximum)	10 Hz/30 min, linear or quadratic drift
Local drift rate (maximum)	0.05 Hz/s
Oscillator noise at constant temperature[a]	0.1 Hz at 1 s, 0.2 Hz at 10 s, 0.4 Hz at 100 s, 0.7 Hz at 1000 s

[a] The oscillator noise figures are based on the specification of the Allan standard deviation of the small deep space transponder, currently under development at JPL.

[13] M. K. Sue, "Preliminary Study Assumptions for the ASMS Study," JPL Interoffice Memorandum 3313-96-MKS02 (internal document), Jet Propulsion Laboratory, Pasadena, California, February 20, 1996.

Appendix B
Glossary of Symbols

The following provides a list of the symbols used throughout this article along with short descriptions of their use:

$a(\nu_k)$ = the Fourier amplitude of random noise, cosine components

$b(\nu_k)$ = the Fourier amplitude of random noise, sine components

$c(\nu_k)$ = the complex Fourier amplitude of random noise

ν_k = the discrete frequency of the Fourier transform

ν_s = the tone frequency of the signal

P(*condition*) = the symbol of mathematical probability

P_D = the probability of detection

P_F = the probability of false alarm

P_{false} = the probability of false detection

P_s = the power of the signal tone

P_n = the power of the thermal noise

P_{s+n} = the power of the amplitude sum of signal and noise

χ^2 = the chi-square probability variable or distribution

σ^2 = the variance of the thermal-noise amplitude

$\Delta\nu$ = the Fourier frequency spacing

η = the power threshold

η_M = the threshold of summed power

$I_{M-1}(z)$ = the modified Bessel function of order $M-1$

M = the number of sequential Fourier transforms used for summing power spectra

N = the number of samples in a Fourier transform

T_s = the sampling interval

T = the integration time of the Fourier transform

N_0 = the constant spectral density of noise

y_0 = the power signal-to-noise ratio

y_{0M} = the total power signal-to-noise ratio

Appendix C

Spectral Power of a Pure Tone Embedded in Noise

In the receiver, a pure spacecraft tone of frequency ν_0, amplitude A, and phase[14] θ may be represented as the sum of the tone and the receiver noise:

$$x(t) = A\cos(2\pi\nu_s t + \theta) + \sum_{k=K_{min}}^{K_{max}} (a(\nu_k)\cos 2\pi\nu_k t + b(\nu_k)\sin 2\pi\nu_k t) \tag{C-1}$$

where the spectral noise coefficients $a(\nu_k)$ and $b(\nu_k)$ are assumed to be white and Gaussian with zero means and variances of σ^2 [10]. The frequency index of the tone signal is denoted by s, which, for simplicity, is assumed to coincide with one of the noise indices. The deviation from this assumption causes signal spread, and this effect will be discussed in Appendix D. The Fourier expansion of the noise is given over a time interval T and, therefore, $\nu_k = k/T$ and $(K_{max} - K_{min})/T = w_r$, where w_r is the frequency bandwidth of the receiving system. Equation (C-1) can be rewritten in complex variables as

$$x(t) = \sum_{k=K_{min}}^{K_{max}} c(\nu_k)e^{i2\pi\nu_k t} + \text{Complex Conjugate} \tag{C-2}$$

where

$$c(\nu_k) = \frac{1}{2}\left(a(\nu_k) - ib(\nu_k) + \delta_{k,s}Ae^{i\theta}\right) \tag{C-3}$$

We can now convert the frequency span of $x(t)$ into a baseband range by multiplying it with orthogonal sinusoid functions with a base frequency ν_b and applying a low-pass filter F with a bandwidth w:

$$\tilde{x}_{\pm}(t) = \begin{cases} F_w[x(t)2\cos 2\pi\nu_b t] \\ F_w[x(t)2\sin 2\pi\nu_b t] \end{cases} \tag{C-4}$$

Then, after an index translation in frequency $k - k_b \rightarrow k$, we get

$$\tilde{x}_{\pm}(t) = \sum_{-k_{max}}^{k_{max}} c_{\pm}(\nu_k)e^{i2\pi\nu_k t} \tag{C-5}$$

Here $\nu_k = k/T$ and $k_{max}/T = w$, where w is the frequency bandwidth of the filter and the following notations were introduced:

[14] In general, the phase may be a function of the time (i.e., phase noise); here it is approximated by a constant.

$$\left.\begin{array}{ll} c_+(\nu_k) = c(\nu_k) & \text{if } k > 0 \\ c_+(\nu_{k)} = c(\nu_k) + c^*(\nu_k) & \text{if } k = 0 \\ c_-(\nu_k) = ic(\nu_k) & \text{if } k > 0 \\ c_-(\nu_{k)} = ic(\nu_k) + (ic(\nu_k))^* & \text{if } k = 0 \\ c_\pm(\nu_{-k}) = c_\pm^*(\nu_k) & \text{for all } k \end{array}\right\} \tag{C-6}$$

Since the two data streams $\tilde{x}_+(t)$ and $\tilde{x}_-(t)$ represent orthogonal components of the Fourier spectrum, both may be sampled at half of the full Nyquist rate (the FSR samples accordingly). If T_s denotes the corresponding double Nyquist sampling interval, then $k_{max} = T/T_s = N$, where N is the number of samples in the time interval T.

The Fourier amplitudes $c_\pm(\nu_k)$ can be expressed as

$$c_\pm(\nu_k) = \frac{1}{T}\int_0^T dt\ \tilde{x}_\pm(t)e^{-i2\pi\nu_k t} \tag{C-7}$$

which, for finite sampling of $\tilde{x}_\pm(t)$, can be approximated by the sum

$$c_\pm(\nu_k) = \frac{1}{N}\sum_{j=1}^{N} \tilde{x}_\pm(t_j)e^{-i2\pi\nu_k t_j} \tag{C-8}$$

This is equivalent to the approximation of the Fourier transform over a finite sampling interval using a finite number of sampling points. The time-averaged power then is given by

$$\begin{aligned} P &= \frac{1}{T}\int_0^T dt\ \frac{1}{2}\left(\tilde{x}_+^2(t) + \tilde{x}_-^2(t)\right) \\ &= \frac{1}{2}\left(c_+^2(0) + c_-^2(0)\right) + \sum_{k=1}^{k_{max}}\left(|c_+(\nu_k)|^2 + |c_-(\nu_k)|^2\right) \\ &= \frac{1}{2}A^2 + \sum_{k=0}^{k_{max}}\frac{1}{2}\left(a^2(\nu_k) + b^2(\nu_k)\right) = \frac{1}{T}\int_0^T dt\ x^2(t) \end{aligned} \tag{C-9}$$

which expresses Parseval's theorem and conservation of power during downconversion. Notice that averaging over both components of downconverted power was necessary to conserve power due to the aberration at zero frequency. All statistical information can now be deduced from the multivariate Gaussian distribution of the coefficients $a(\nu_k)$ and $b(\nu_k)$, which are independent variables with zero mean. If we assume a flat single-sided power spectrum density N_0, then the time and ensemble-averaged power of single Fourier components becomes

$$\langle P_k \rangle = \delta_{k,0} \frac{1}{2} A^2 + N_0 \frac{1}{T} \tag{C-10}$$

since the bandwidth of a single Fourier component is $1/T$, $k_{max}/T = w$ as noted above, and $(1/2)(a^2(\nu_k) + b^2(\nu_k)) = N_0/T$. Equation (C-11) below is then the sum of the time and ensemble-averaged power of single Fourier components:

$$\begin{aligned} \langle P \rangle &= \frac{1}{2} A^2 + \sum_{k=0}^{k_{max}} N_0 \frac{1}{T} \\ &= \frac{1}{2} A^2 + N_0 w \end{aligned} \tag{C-11}$$

Thus, denoting the signal power as $P_s = (1/2)A^2$, the signal-to-noise ratio at the tone frequency becomes $(P_s/N_0)T$.

Appendix D
Spectral Interpolation

The discrete Fourier transform is defined over a set of fixed frequencies while the actual tone frequency will not fall on one of the fixed discrete frequencies. As a result, the power spectrum of the tone spreads over all Fourier frequencies, and the observed peak spectral power is less than the original power of the tone. For a given tone frequency ν_s and Fourier integration time T, the signal power at the discrete Fourier frequency ν_k is $\mathrm{sinc}^2(\pi(\nu_k - \nu_s)T)$.[15] The worst case is when the tone lies exactly between two Fourier frequencies, $|\nu_k - \nu_s| = 1/2T$; the two peak powers are then reduced by 4 dB as compared with the original tone power. This effect can be partially removed by either interpolation of the Fourier spectrum or by shifting the tone frequency of the signal closer to the discrete Fourier frequency.

The Fourier spectrum is interpolated by "zero-padding" the data by adding a sequence of fake samples with zero value to the end of the sequence of observed samples prior to the Fourier transform. As the duration of the Fourier transform increases, the number of Fourier frequencies also increases for a fixed bandwidth. This has the effect of decreasing the frequency difference $|\nu_k - \nu_s|$, while T remains unchanged in the $\mathrm{sinc}^2(\pi(\nu_k - \nu_s)T)$ function. If the data are zero padded by a factor of two, i.e., N zero-valued samples are appended to N observed samples, the maximum power loss due to signal misalignment with the Fourier frequencies is $10 \log \mathrm{sinc}^2(\pi/4) = -0.9$ dB; zero padding by a factor of four reduces the maximum loss to $10 \log \mathrm{sinc}^2(\pi/8) \approx -0.2$ dB. These Fourier-transform interpolated-resolution improvements come, of course, at the expense of increased computation as well as increased complexity of statistical considerations. As a compromise, zero padding by two was used in the evaluation of experimental data.

The average power loss can be calculated by integral averaging the gain function $\mathrm{sinc}^2(\pi\nu/\Delta\nu)$ over the interpolated resolution:

$$G_m = \frac{2k}{\Delta\nu} \int_0^{\Delta\nu/2k} d\nu \, \mathrm{sinc}^2 \frac{\pi\nu}{\Delta\nu} = \frac{2k}{\pi} \int_0^{\pi/2k} dx \, \left(\frac{\sin x}{x} \right)^2 \tag{D-1}$$

where k is the factor of zero padding. Expanding the integrand in a Taylor series gives

$$G_m = \frac{2k}{\pi} \int_0^{\pi/2k} dx \, \left(1 - \frac{1}{3}x^2 + \frac{2}{45}x^4 \ldots \right) = 1 - \frac{1}{9}\left(\frac{\pi}{2k}\right)^2 + \frac{2}{225}\left(\frac{\pi}{2k}\right)^4 \ldots \tag{D-2}$$

Therefore, for a zero padding by a factor of two, the average power loss is ≈0.3 dB.

The alternate method is frequency shifting of the tone. In this case, two or multiple baseband conversions are performed at the frequencies of ν_b, $\nu_b + \Delta\nu/2$, $\nu_b + \Delta\nu/4$, etc., where ν_b is the baseband frequency. Processing each baseband data stream then yields estimates of the signal power. The optimum of these powers is selected, giving estimates of the signal power and frequency. This method requires an increased amount of computations; however, the process can be streamlined somewhat for computational efficiency.

[15] $\mathrm{sinc}\ x = \sin x / x$.

Appendix E

Power Loss Due to Frequency Drifts: Estimation of the Integration Time of Fourier Transforms

We consider two kinds of oscillator frequency drifts: a long-term drift caused by temperature changes (this is subsequently modeled by a linear function) and the stochastic frequency noise of the oscillator.[16] Although these are simultaneous effects, we first consider them separately. The determination of the optimum value of the integration time T is performed in iterative steps. In the first step, a crude statistical estimate is given from power loss considerations, and then the value of T is chosen. In the second step, an approximate value of the signal power-loss is calculated for the chosen T.

The constraint that the frequency drift no more than one-quarter of the Fourier-frequency spacing, $\Delta\nu$, during the integration time, T, implies $\Delta\nu/T > 4\dot{\nu}$ and, since $\Delta\nu = 1/T$, thus, $T < 1/\sqrt{4\dot{\nu}}$. According to the ASMS specifications, $\dot{\nu} = \pm 0.05$ Hz/s; thus, $T < 2.2$ s. However, besides the linear drift, the oscillator fluctuates at the 0.1-Hz level at an integration time of 1 s, and the fluctuation level is higher at larger integration times (Appendix A). By denoting the standard deviation of the oscillator fluctuation by $\sigma_{osc}(T)$, the drift range condition above implies that, for a 3σ confidence level, $3\sigma_{osc} < 1/4T$ and, thus, $T < 1/(12\sigma_{osc}(T))$. Using the 1-s specification for noise, we get $T < 0.83$ s. If we superimpose the noise on the linear drift, then the presence of fluctuation increases the drift, the equivalent extreme drift rate can be approximated by $\dot{\nu} + 3\sigma_{osc}(T)/T$, and, therefore,

$$\dot{\nu} + \frac{3\sigma_{osc}(T)}{T} < \frac{1}{4T^2} \tag{E-1}$$

This implies that

$$T < \frac{\sqrt{9\sigma_{osc}^2(T) + \dot{\nu}} - 3\sigma_{osc}(T)}{2\dot{\nu}} \tag{E-2}$$

and, thus, $T < 0.74$ s. These simple statistical considerations largely coincide with our experimental observation on the spare oscillator of the Galileo spacecraft; the detection performance degrades over a few seconds of integration time.

Now we are in a position to calculate the actual power loss due to tone-frequency fluctuation. Based on the above estimates, we choose $T = 1s$. The frequency gain function of the tone is

$$G_\nu(\nu T) = \mathrm{sinc}^2 \frac{\pi\nu}{\Delta\nu} \approx 1 - \frac{\pi^2}{3}\left(\frac{\nu}{\Delta\nu}\right)^2 \tag{E-3}$$

By averaging over the frequency fluctuation, we get

$$\langle G_\nu(\nu T)\rangle = 1 - \frac{\pi^2}{3}(\sigma_{osc}(T)T)^2 \tag{E-4}$$

Since $\sigma_{osc}(1\mathrm{s}) = 0.1$ Hz/s, the loss due to the frequency fluctuation is $10\log\left(1 - (\pi^2/3)0.1^2\right) \approx -0.15$ dB.

[16] There also is a residual Doppler frequency drift due to spacecraft-trajectory modeling errors. For a deep-space probe, this effect is ignorable in comparison with the oscillator drifts.

The average power loss due to the linearly drifting tone frequency is calculated by frequency-rate averaging the power of the Fourier amplitude of the drifting signal at zero frequency;[17] thus, the frequency-rate gain function is

$$G_{\dot\nu}(\dot\nu T^2) = \frac{1}{\dot\nu}\int_0^{\dot\nu} d\dot f \left| \frac{1}{T}\int_0^T dt\ \exp\frac{i2\pi\dot f t^2}{2} \right|^2 \tag{E-5}$$

Expanding the inner integrand into a Taylor series and performing the integral, we obtain

$$G_{\dot\nu}\left(\dot\nu T^2\right) = \frac{1}{\dot\nu}\int_0^{\dot\nu} d\dot f \left| 1 + i\frac{\pi\dot f T^2}{3} - \frac{\left(\pi\dot f T^2\right)^2}{10}\ldots \right|^2 \tag{E-6}$$

Collecting the lowest order of corrections and performing the integral over $\dot f$, the final result is

$$G_{\dot\nu}(\dot\nu T^2) = 1 - \frac{4\pi^2}{3{\cdot}45}\left(\dot\nu T^2\right)^2 \tag{E-7}$$

Substituting the ASMS value, $\dot\nu = 0.05$ Hz/s, and setting $T = 1$ s, we get the final estimate of the power loss due to linear-frequency drifting of the tone: $10\log(1 - (4\pi^2/135)0.05^2) = -0.003$ dB.

[17] In general, the gain function is evaluated for the complete frequency-drift function, and it is averaged over all parameters simultaneously. The first-order cross term vanishes for symmetric averaging; that is the reason for evaluating Eq. (E-5) at the zero frequency. The contribution of the higher-order cross terms is ignorable here.